Sci. Bull.
DOI 10.1007/s11434-016-1143-6

www.scibull.com
www.springer.com/scp

Review

Engineering Sciences

The constant-volume propagating spherical flame method for laminar flame speed measurement

Mahdi Faghih · Zheng Chen

Received: 3 April 2016 / Revised: 28 May 2016 / Accepted: 17 June 2016

Abstract Laminar flame speed is one of the most important intrinsic properties of a combustible mixture. Due to its importance, different methods have been developed to measure the laminar flame speed. This paper reviews the constant-volume propagating spherical flame method for laminar flame speed measurement. This method can be used to measure laminar flame speed at high pressures and temperatures which are close to engine-relevant conditions. First, the propagating spherical flame method is introduced and the constant-volume method (CVM) and constant-pressure method (CPM) are compared. Then, main groups using the constant-volume propagating spherical flame method are introduced and large discrepancies in laminar flame speeds measured by different groups for the same mixture are identified. The sources of discrepancies in laminar flame speed measured by CVM are discussed and special attention is devoted to the error encountered in data processing. Different correlations among burned mass fraction, pressure, temperature and flame speed, which are used by different researchers to obtain laminar flame speed, are summarized. The performance of these correlations are examined, based on which recommendations are given. Finally, recommendations for future studies on the constant-volume propagating spherical flame method for laminar flame speed measurement are presented.

M. Faghih · Z. Chen (✉)
State Key Laboratory for Turbulence and Complex Systems (SKLTCS), Department of Mechanics and Engineering Science, College of Engineering, Peking University, Beijing 100871, China
e-mail: cz@pku.edu.cn

Keywords Laminar flame speed · Propagating spherical flame · Constant-volume method · Burned mass fraction · Methane/air

1 Introduction

Laminar flame speed, S_u^0, is an important intrinsic property of a combustible mixture. It is defined as the speed at which an adiabatic, unstretched, premixed planar flame propagates relative to the unburned mixture [1]. Laminar flame speed contains the physicochemical information about the mixture's diffusivity, reactivity, and exothermicity. It affects or even determines the burning rate of fuel/air mixtures in practical combustion systems [2]. Besides, many premixed flame phenomena, such as extinction, flash back, and blow off can be characterized by S_u^0 as a reference parameter [3]. In fundamental combustion research, S_u^0 is an important target for the validation of chemical mechanisms and for development of surrogate fuel models (e.g., [4–6]). Accurate flame speeds measured at high pressures and temperatures are very useful for developing/validating kinetic mechanisms of fuels. Furthermore, S_u^0 is popularly used as a scaling parameter for turbulent flame speed; and it is used in certain turbulent premixed combustion modelling [7].

Due to the importance of S_u^0, great attention has been paid to its *accurate* measurement. As reviewed in Refs. [1, 8, 9], several experimental approaches have been developed to measure S_u^0 using different flame configurations, including Bunsen flame [10], counter flow or stagnation flame [11–14], burner stabilized flat flame [15, 16], and outwardly propagating spherical flames [2, 8, 10, 17–32].

The Bunsen flame method was introduced by Bunsen [33]. This method was very common in the first century of

Published online: 09 July 2016

its introduction due to its simplicity and well defined structure. However, in recent years, it has been realized that Bunsen flame is affected by different factors such as flame instability, stretch, curvature and heat loss [34, 35]. Counter flow flame or stagnation flame was introduced in Ref. [36] and then it was used to measure S_u^0 [12]. The advantage of this method is that the influence of stretch on flame speed can be quantified and extracted by using the procedure proposed by Wu and Law [12]. However, it is difficult to use this method at pressures above 5 atm (1 atm = 1.013×10^5 Pa) [9]. The burner-stabilized flat flame method was first proposed by Botha and Spalding [37]. Later de Goey et al. [38] proposed the so-called heat flux method to measure S_u^0 from burner-stabilized flat flame. It has the advantages in circumventing the heat loss issue in burner stabilized flat flame. The drawbacks of heat flux method are the uncertainty of the method due to radiation, boundary condition effect at the burner surface, catalytic effect of the metal surface, flame instability and flow disturbance from the burner holes [9, 39]. It is also difficult to use the heat flux method at high pressures.

According to above discussion, it is difficult to use Bunsen flame, stagnation flame, and burner-stabilized flat flame to measure S_u^0 at high pressures. Currently, the propagating spherical flame method, which will be introduced in the next section, is the only method which can measure S_u^0 at high pressure close to that in internal combustion engines and gas turbines (20–50 atm) [40].

Several excellent review papers [1, 8, 9] have been published on laminar flame speed measurement. However, unlike other methods, the constant-volume propagating spherical flame method has received little attention. As shall be discussed in the next section, the constant-volume propagating spherical flame method is the only available method to measure S_u^0 at simultaneously high temperatures and high pressures close to engine-relevant conditions. Therefore, this review is focused on the constant-volume propagating spherical flame method. It is noted that a thorough review for this method was given by Rallis and Garforth [8]. However, for the constant-volume propagating spherical flame method, there are several correlations in Refs. [29, 41–49] which can be used to obtain S_u^0 during data processing. It is still not clear which correlation is the most accurate and reliable in terms of S_u^0 determination. The present paper is a contribution to examine and review the performance of these correlations and to clarify the strength and weakness of different correlations.

2 The propagating spherical flame method for S_u^0 measurement

Using propagating spherical flame method to measure S_u^0 goes back to 1920s when the soap bubble method was first introduced by Stevens [50]. In this method, a spherical flame propagates outwardly after central spark ignition in quiescent homogeneous combustible mixture [8, 10]. As shown in Fig. 1, the flame front history or pressure history is recorded, based on which S_u^0 can be determined. At the early stage of flame propagation, the flame curvature/stretch effects are considerable; and the pressure rise is negligible. Later the pressure rise rate increases greatly and the curvature/stretch effects become negligible [51]. Depending on the chamber design as well as the pressure rise, there are two different methods for S_u^0 measurement by using propagating spherical flames: one is the constant-pressure method (CPM) and the other one is the constant-volume method (CVM). Figure 1 schematically describes and compares these two methods. As indicated by the dashed ellipses in Fig. 1, flames with small radii (e.g., $1 \leq R_f \leq 2$ cm) are used in CPM so that the pressure rise is negligible; conversely in CVM since discernable pressure rise is required data corresponding to relatively large flame radii are used.

The constant-pressure propagating spherical flame method (CPM) was first used by Ellis [52] in 1928 who investigated the confinement effect on flame shape in a spherical glass chamber. In CPM, high-speed schlieren or shadow photograph is used to record the flame front propagation [53, 54], from which the evolution of flame radius, $R_f = R_f(t)$, is obtained. When the pressure rise is negligible, the burned gas can be assumed to be static and thus the flame speed relative to burned gas is $S_b = dR_f/dt$. Extrapolation to zero stretch rate is conducted to obtain the unstretched flame speed with respect to burned gas, S_b^0. Finally, the laminar flame speed is determined through $S_u^0 = \sigma S_b^0$, where $\sigma = \rho_b/\rho_u$ is the density ratio between burned and unburned gases [55, 56]. There are two main advantages of CPM [51]: (1) direct view from schlieren/shadow photograph helps to identify the flame instability, which thereby can be prevented in data processing; (2) there exists a quasi-steady spherical flame propagation period during which the stretch effect can be eliminated through extrapolation to zero stretch rate. In the literature, there are extensive studies on S_u^0 measurement using the CPM. The readers are referred to Refs. [9, 57, 58] and references therein for more details.

The constant-volume propagating spherical flame method (CVM) was first used in 1934 by Lewis and von Elbe [49]. In CVM, outwardly propagating spherical flames occur in a closed thick-walled spherical vessel and the evolution of chamber pressure rather than flame radius is recorded. Figure 1 shows that the pressure rise is evident only when the flame radius is large enough. The recorded pressure history is then used to determine S_u^0 through correlations between S_u^0, pressure, pressure rise rate, and burned mass fraction. This method has the advantage that S_u^0 for a given mixture over a wide range of pressures and

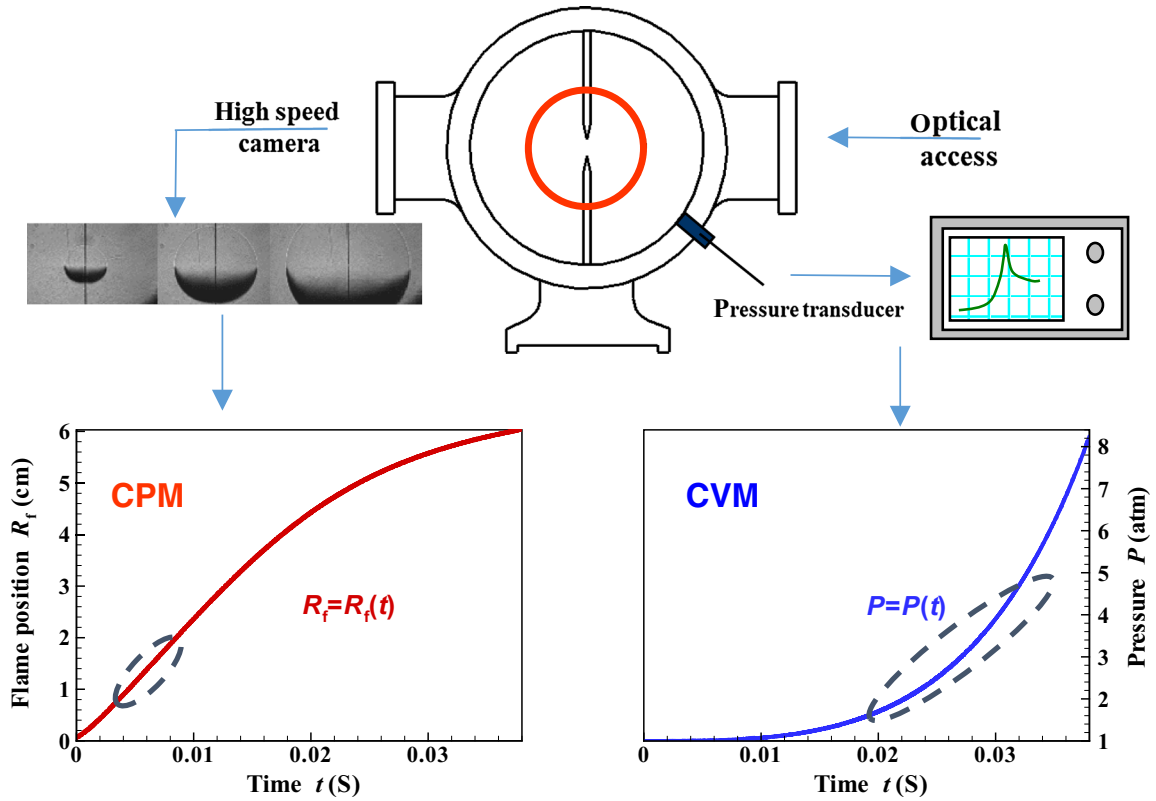

Fig. 1 (Color online) Schematic for the constant-pressure method (CPM) and constant-volume method (CVM) using propagating spherical flames. The results in the two figures above were obtained from simulation for stoichiometric methane/air initially at normal temperature and pressure (NTP) and in a spherical chamber of 6 cm in radius

temperatures can be simultaneously measured from a single test [8]. Moreover, it is possible to use CVM to measure S_u^0 in engine-relevant pressures and temperatures of 50–70 atm. and 700–800 K [40]. However, CVM has the disadvantage that the possible appearance of flame instability is not identified and thereby the accuracy in S_u^0 measurement may be reduced.

Both CPM and CVM have been used to measure S_u^0 at high pressures [59, 60]. Because of the requisite of optical access, the upper pressure limit of CPM is usually lower than that of CVM. However, dual chambers have been used to develop the pressure-release type high-pressure combustion facilities [17, 20] and pressures up to 60 atm have been reached for the CPM. The outer chamber is filled with an inert mixture and thus flame propagation terminates as it reaches the wall of the inner vessel. Therefore, excessive pressure buildup can be prevented using dual chambers. Compared to CVM, the main drawback of CPM is its relatively low temperature ranges [40]. To increase the initial temperature, both electrical heating [61] and external heating oven [62] can be used which enable to increase the initial temperature to 500 K. In the external heating oven, an electrical fan is incorporated to keep the non-uniformity of temperature below 5 K. Electrical heating is also used to increase the initial temperature of the vessel in CVM [63]. For CPM, a pair of windows need to be embedded on the surface of combustion chamber. Consequently, it is impossible to conduct spherical flame experiments at simultaneously high pressure and high temperature ranges by CPM, and the temperature cannot reach the value close to engine-relevant conditions [40]. Unlike CPM, CVM does not require optical access and experiments can be conducted in a completely closed chamber. Therefore, as pointed out by Xiouris et al. [40], very high pressure and temperature close to engine-relevant conditions can be reached by CVM for realistic liquid fuels. Compared to other methods, CVM was considered to be "the most versatile and accurate" by Rallis and Garforth [8]. Therefore, this review is focused on CVM.

3 Experiments and discrepancies in S_u^0 measurement using the CVM

Both experiments and simulations can be conducted to obtain S_u^0 using CVM. However, direct numerical simulations of outwardly propagating spherical flames in a close chamber with large pressure rise were only conducted by

Chen et al. [51, 64] and Xiouris et al. [40]. Different groups including Iijima and Takeno [45], Sharma et al. [65], Farrel et al. [66], Yates et al. [67] and Matsugi et al. [68] used CVM in their experiments. The main groups thoroughly investigated S_u^0 measurement by CVM experiment are Metghalchi et al. [2, 31, 42, 60, 69–72], Stone et al. [30, 44, 73–77] and Razus et al. [41, 63, 78, 79]. Before 2001, Metghalchi's group only used a spherical chamber to measure the pressure evolution [2, 60]. After 2001, they used both spherical and cylindrical vessels. The cylindrical vessel with optical access is used to identify possible instability and cellular formation in flame front [31, 42, 69–72]. Consequently, S_u^0 obtained from CVM is not affected by flame instability. Cellular formation is a concern for lean H_2/air mixture in which thorough investigation of cellularity is necessary by optical access [80]. Stone and coworkers used a spherical vessel with optical access so that both pressure history and flame front history were recorded in experiments [30, 44, 73]. Similar to Metghalchi's group, Stone's group used flame front history data to analyze flame instability and used pressure history to get S_u^0 by CVM. However the optical access in their spherical chamber limited the peak pressure which can be reached in experiments. Unlike these two groups, Razus et al. [41, 63] only measured the pressure history and no optical access was available in their spherical chamber. Table 1 summarizes the characteristics of CVM experiments performed by different groups to measure S_u^0.

Although CVM has been popularly used by many groups, there are still large discrepancies in S_u^0 measured by different groups for the same mixture at nearly the same condition. Figure 2 shows the results measured for CH_4/air at normal temperature and pressure (NTP, 298 K and 1 atm) by different groups [45, 65, 66, 72, 75, 76] using CVM (data measured from CPM for CH_4/air at NTP were compared in Ref. [58] and thereby were not repeated here). The results predicted by CHEMKIN–PREMIX code [81] based on GRI-Mech. 3.0 [82] are plotted together for comparison. Smaller scatter is observed for near-stoichiometric mixtures; while larger scatter is observed for off-stoichiometric mixtures. To quantify the discrepancies in S_u^0 measured from CVM, Fig. 3 shows the deviation of S_u^0 measured by different groups [45, 65, 66, 72, 75, 76] from that predicted by simulation, $S_{u,PREMIX}^0$ [81]. Even for stoichiometric CH_4/air, the difference among normalized values of $S_u^0/S_{u,PREMIX}^0$ is around 18 %. For very lean and rich CH_4/air mixtures, the maximum difference is much larger: 29 % and 28.5 % for $\phi = 0.6$ and 1.3, respectively. It is noted that due to the lack of enough experimental data for these two extreme equivalence ratios, the experiment results are compared to simulation results.

As mentioned before, S_u^0 measured from CVM can be used to validate and develop chemical kinetic models. However, the experimental data are useful only when the uncertainty in S_u^0 measurement is lower than the uncertainty in kinetic models. Figure 4 shows the sensitivity-weighted uncertainty momentum for S_u^0 of CH_4/air at NTP [58]. It is observed that the sensitivity-weighted uncertainty momentum of main elementary reactions is comparable to the relative discrepancy in S_u^0 measurement indicated by Fig. 3. To restrain the uncertainty of chemical models, the lower the uncertainty in experimental S_u^0 measurement, the more useful of these data. Therefore, efforts are still need to be devoted to improving the accuracy of S_u^0 measurement using the CVM.

Chen [58] reviewed different sources of uncertainty in S_u^0 measurement using the CPM. Due to the similarity between CVM and CPM, most of the uncertainty sources in CPM are also important in CVM. The possible sources of uncertainty in CVM are mixture preparation [9, 83, 84], ignition [24, 57, 85, 86], buoyancy [87, 88], instability [20, 89, 90], confinement [51, 91–93], radiation [93–98], stretch [51] and data processing. Xiouris et al. [40] introduced a method to quantify the uncertainty of S_u^0 measurement in CPM experiments. The method considers uncertainty from three stages: mixture preparation, data acquisition and data processing. Each of these stages are treated separately and the accumulative uncertainty of these steps is calculated in final step [40]. Similar procedure was used in Ref. [40] to assess the uncertainty in S_u^0 measured by CVM.

For mixture preparation, while negligible uncertainty is anticipated from initial pressure variation, the uncertainty for initial temperature variance of ±3 K is around 2 % and it reaches to 2.5 %–4 % for initial temperature variance of ±5 K for CH_4/air at NTP [58]. The uncertainty in equivalence ratio strongly depends on the accuracy of pressure gauge (usually the mixture is prepared using the partial pressure method). For CH_4/air at NTP and in lean and rich cases of $\phi = 0.6$ and 1.4, the uncertainty of S_u^0 measurement is around 6 % when very accurate pressure gauges with accuracy of ±0.05 % are used; while it reaches to 10 % when normal or low accuracy of ±0.25 % pressure gauges are used [58]. To measure S_u^0 for liquid fuels, heating is used to evaporate the liquid fuel before entering the combustion chamber [42, 70]. For liquid fuels, the heating and vaporization of fuels also bring uncertainty in the mixture composition [58].

In CVM, the ignition effect is negligible since data processing is conducted for flames with obvious pressure rise rate. The buoyancy effect is negligible for mixtures with $S_u^0 > 15$ cm/s [87] but it cannot be neglected for highly diluted mixtures, for which micro-gravity experiments are needed [88]. In Refs. [40, 99] radiation effects on laminar flame speed measurement in propagating spherical flames were investigated thoroughly. Xiouris et al. [40] found that neglecting radiation heat loss when interpreting experimental data in CVM can result in uncertainty as large

Table 1 The characteristics of CVM experiments performed by different groups to measure S_u^0

Group	Mixture	Vessel type and size	Method incorporated
Metghalchi and Keck [2, 60]	C_3H_8, CH_3OH, C_8H_9N and C_8H_{18} in air	Spherical chamber/diameter: 15.24 cm	A formula based on correction factor and flame front area/CVM
Metghalchi et al. [72]	CH_4/diluent/air	Spherical chamber/diameter: 15.24 cm	Multi-zone model, in house code/Eq. (11) and Markstein length is used to find S_u^0/CVM
Metghalchi et al. [31, 42, 69–71]	CH_4/O_2/Ar, JP-10/air, C_2H_6O/diluent/air, $C_{10}H_{22}$/air, HFC-32/air, HFC-152a/air	(a) Cylindrical chamber with optical access: to investigate shape of flame (b) Spherical chamber/diameter: 15.24 cm to find laminar flame speed	Multi-zone model, in house code/Eq. (11), stretch rate is neglected/both CVM and CPM
Stone et al. [76]	CH_4/diluent/air	Spherical chamber/diameter: 15 cm	Two-zone model, Eqs. (14), (22) and (26) are used to find S_u^0/CVM
Stone et al. [30, 73–75]	CH_3OH, CH_4, C_4H_{10}, C_7H_{16}, C_8H_{18} C_7H_8, $C_6H_5CH_2CH_3$, C_2H_6O and biogas in air	Spherical chamber/diameter: 16 cm; both optical access and pressure transducer are provided for the same experimental facility	Multi-zone model (BOMB) program and Eq. (25); stretch rate is neglected in sufficient pressure rise/both CVM and CPM
Razus et al. [63, 78]	C_3H_8/air and C_2H_6/air	Spherical chamber/diameter: 10 cm; merely pressure transducer was used	Two-zone model, Eqs. (10), (15), (21) and stretch rate is neglected for $P > 1.5P_0$/CVM
Matsugi et al. [68]	$H_2/NF_3/N_2$, $CH_4/NF_3/N_2$, and $C_3H_8/NF_3/N_2$	Spherical chamber/diameter: 15.29 cm; both optical access and pressure transducer are provided for the same experimental facility	Two-zone model, Eqs. (10), (14) and (26) are combined and Markstein length is used to find S_u^0/both CVM and CPM
Xiouris et al. [40]	Synthesis gas, CH_4/air and C_3H_8/air	(a) Cylindrical chamber with optical access: to investigate thermal-diffusivity and hydro-dynamic instabilities (b) Spherical chamber/diameter: 20.32 cm to find laminar flame speed	Multi-zone model, both DNS (TORC) and experiment are used/Eq. (6) and stretch rate is neglected for $P > 2.5P_0$ both CVM and CPM

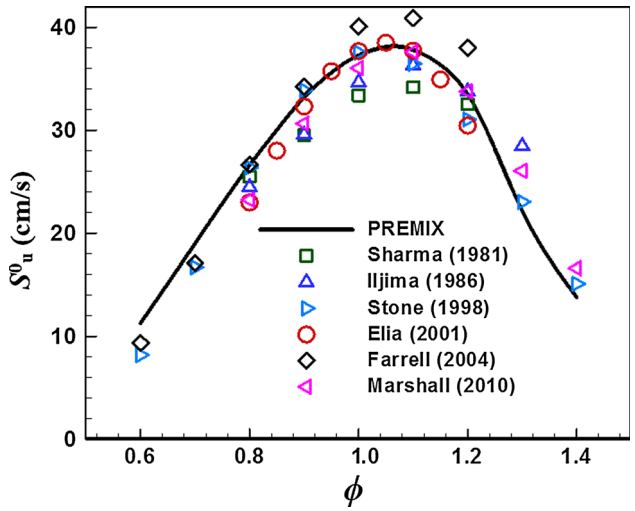

Fig. 2 (Color online) Laminar flame speed of CH_4/air at NTP. The symbols denote experimental results measured from CVM [45, 65, 66, 72, 75, 76]. The line denotes numerical results predicted by GRI-Mech. 3.0 [82] using CHEMKIN–PREMIX code [81]

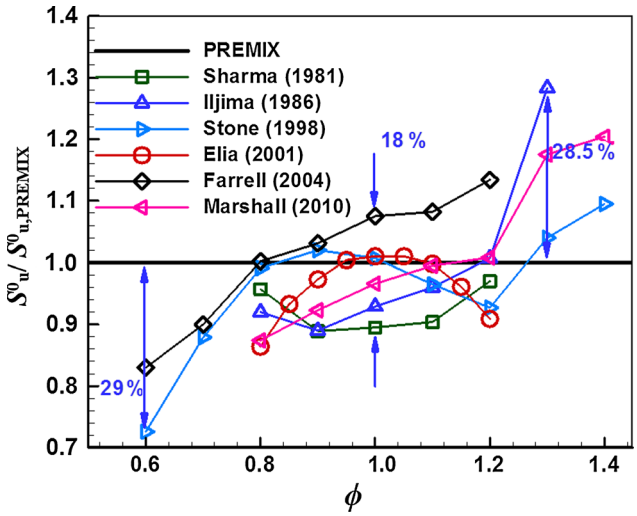

Fig. 3 (Color online) Deviation of S_u^0 measured by different groups [45, 65, 66, 72, 75, 76] from $S_{u,PREMIX}^0$ predicted by simulation based on GRI-Mech. 3.0 [82]

as 15 % and they proposed a method to account for this. For CO_2 diluted mixtures, radiation absorption was found to play an important role and the radiation induced uncertainty is negligible for CPM [99]. The radiation effect increases greatly as S_u^0 decreases [97]. For CH_4/air at NTP and with the equivalence ratio in the range of 0.7–1.3, the radiation-induced uncertainty in S_u^0 measurement is around 3 %; and it reaches 5 % for very lean or rich cases of $\phi = 0.7$ or 1.4. For near lean flammability mixture ($0.5 < \phi$

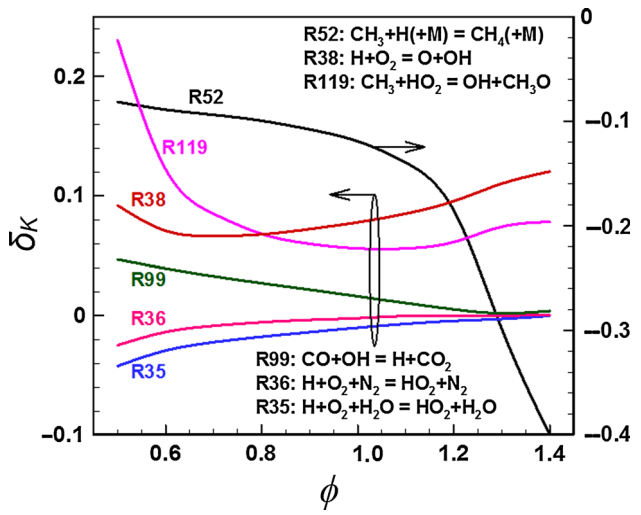

Fig. 4 (Color online) Sensitivity-weighted uncertainty momentum, δ_K, as a function of equivalence ratio for S_u^0 of CH_4/air at NTP. $\delta_K = S_K \times (f_K - 1)$ and f_K is the uncertainty factor of Kth elementary reaction ($f_K = 1.2$ for R35, R36, R38, and R99; $f_K = 2.0$ for R119; $f_K = 4.0$ for R52). Figure adapted from Ref. [58]

< 0.6), the radiation-induced uncertainty is above 6 %. The stretch effect was investigated by Chen et al. [51] and it is negligible when the relative pressure rise is above 20 %. The shape and size of combustion vessel can also affect the measurement using CVM. Unlike CPM, spherical vessel should be used for CVM experiments. Besides, data processing should be conducted for $P > 2.5P_0$ [40] so that the ignition and stretch effects are negligible. Therefore, the combustion vessel should not be too small; otherwise enough data cannot be measured before flame reaches the wall. Dahoe [100] conducted the CVM experiments in small cylindrical vessel (169 mL) for H_2/air mixture and observed oscillation in the pressure–time curve of hydrogen–air deflagration. The oscillation is due to cylindrical shape and small diameter of combustion vessel. Ma et al. [101] conducted similar experiments in a 20 L spherical vessel and Salzano et al. [102] conducted experiments in a 5 L cylindrical combustion vessel but they did not find any oscillation in pressure-time history. The last and the most important factor affecting the accuracy of S_u^0 measurement from CVM is data processing. There are different correlations among pressure, temperature, burned mass fraction and flame speed, which are used by different researchers to obtain S_u^0. These correlations and their performance are introduced in the next section.

4 Determination of S_u from CVM

Since the influence of stretch on laminar flame speed is usually neglected in CVM [42, 69, 73, 78], in this section we use S_u instead of S_u^0 to denote laminar flame speed. Recently Xiouris et al. [40] confirmed this assumption in their experiments and simulations, for pressure above two and a half times of the initial pressure.

4.1 Assumptions and basic equations

In CVM, S_u is determined based on the following assumptions [8]: (1) the spherical flame front is smooth and free from diffusion-thermal and hydrodynamic instabilities; (2) both the unburned and burned gases are ideal; (3) the pressure is uniformly distributed in the whole combustion vessel; (4) the unburned gas is compressed isentropically; (5) there is no dissociation or pre-flame reaction in the unburned gas; (6) chemical equilibrium is reached immediately behind the flame front, and (7) the radiation and buoyancy effects are negligible.

Figure 5 schematically shows the flame propagation in a closed spherical vessel. The spherical flame with the radius of R_f is assumed to be ultimately thin and it separates the burned and unburned gas regions. According to mass conservation, we have

$$m_0 = m_u + m_b, \tag{1}$$

where the subscripts "0", "u" and "b" denote the initial states and states of unburned and burned gases, respectively, and m stands for mass. From Eq. (1), we have

$$\frac{dm_u}{dt} = -\frac{dm_b}{dt}. \tag{2}$$

According to the definition of laminar flame speed, we have

$$\frac{dm_u}{dt} = -4\pi R_f^2 \rho_u S_u, \tag{3}$$

in which ρ_u is the density of unburned gas. The mass of unburned gas is $m_u = 4\pi(R_W^3 - R_f^3)\rho_u/3$, where R_W is the

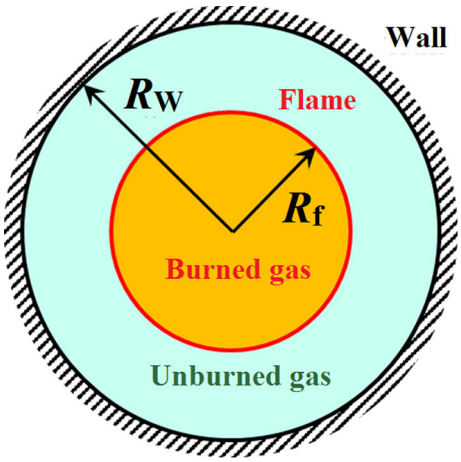

Fig. 5 (Color online) Schematic sketch of spherical flame propagating in a closed spherical vessel

inner radius of the spherical chamber. Therefore, Eq. (3) becomes

$$S_u = \frac{dR_f}{dt} - \frac{R_W^3 - R_f^3}{3R_f^2\rho_u}\frac{d\rho_u}{dt}. \quad (4)$$

Since the unburned gas is compressed isentropically, we have

$$\rho_0/\rho_u = (P_0/P)^{1/\gamma_u}. \quad (5)$$

Substituting Eq. (5) into (4) yields

$$S_u = \frac{dR_f}{dt} - \frac{R_W^3 - R_f^3}{3P\gamma_u R_f^2}\frac{dP}{dt}. \quad (6)$$

We introduce the burned mass fraction (BMF) defined as $x = m_b/m_0$. Therefore, Eq. (1) becomes

$$m_u = (1-x)m_0, \quad (7)$$

which indicates that

$$\frac{4\pi}{3}\left(R_W^3 - R_f^3\right)\rho_u = (1-x)\frac{4\pi}{3}R_W^3\rho_0. \quad (8)$$

Substituting Eq. (5) into (8) yields the following relationship between flame radius and pressure

$$\frac{R_f}{R_W} = \left[1 - (1-x)\left(\frac{P_0}{P}\right)^{1/\gamma_u}\right]^{1/3}. \quad (9)$$

Substituting Eq. (9) into (6) yields

$$S_u = \frac{R_W}{3}\left(1 - (1-x)\left(\frac{P_0}{P}\right)^{1/\gamma_u}\right)^{-2/3}\left(\frac{P_0}{P}\right)^{1/\gamma_u}\frac{dx}{dt}, \quad (10)$$

which is the formulation widely used to determine S_u in CVM. In this equation, BMF needs to be determined as a function of pressure measured in experiments, i.e., $x = x(P)$. This can be determined by the two-zone or multi-zone models discussed in the next subsection.

4.2 Two-zone and multi-zone models

Two-zone and multi-zone models are used in CVM formulation [43, 44, 72, 78]. In both models the flame is assumed to be infinitely thin. The pressure is uniformly distributed in the whole domain, which is confirmed by simulation results shown in Fig. 6a for stoichiometric CH_4/air mixture. In both models, the unburned gas is chemically frozen and compressed isentropically by the propagating spherical flame [43]. In the multi-zone model, a thermal boundary layer near the wall can be considered in which heat loss occurs through the surrounding wall [71, 72].

The main difference between two-zone and multi-zone models is the treatment of burned gas. In the two-zone model, the burned gas is assumed to have the same properties and the temperature gradient in burned gas is neglected. In multi-zone model, the burned gas is divided to multiple shells. While the temperature gradient is zero in each shell, it differs from shell to shell and consequently there is temperature gradient in the whole burned gas region. In the two-zone model, neglecting the temperature gradient in burned gas imposes some errors in evaluating the BMF which is a crucial parameter to obtain S_u by CVM. Figure 6b shows the temperature distributions from numerical simulation. It is observed that before $t_{15} = 15$ ms, the temperature gradient in burned gas is relatively small. However, obvious temperature gradient occurs in burned gas during the spherical flame propagating toward the wall. Similar results were obtained in experiments [30] and the temperature difference in burned gas region between the inner shell and the outmost shell was found to reach 500 K.

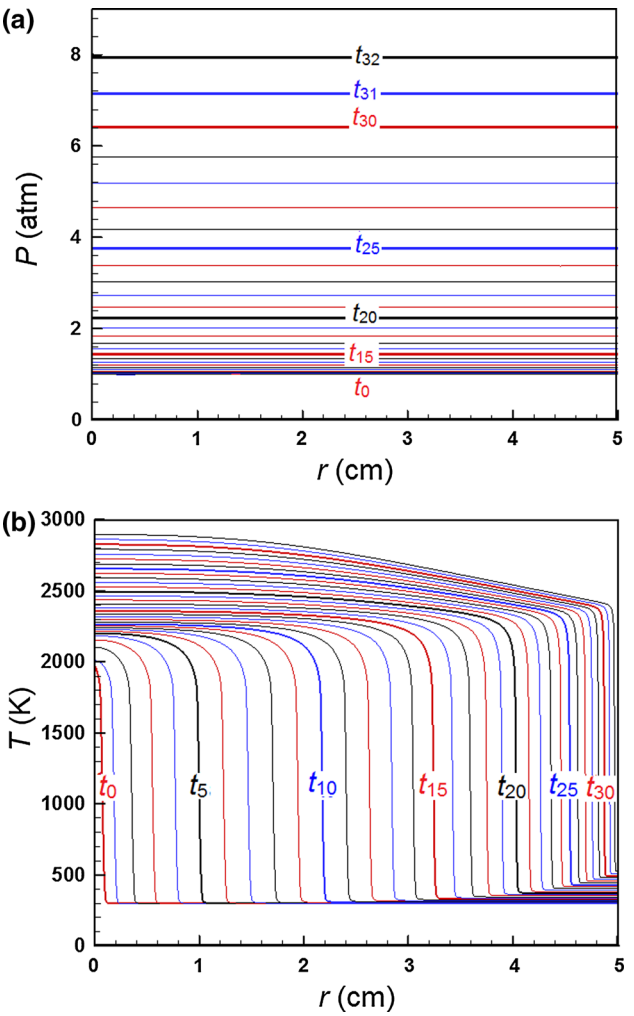

Fig. 6 (Color online) The evolution of pressure (**a**) and temperature (**b**) distributions for stoichiometric CH_4/air initially at NTP

Metghalchi et al. [72] developed a multi-zone model for CVM. In their multi-zone model, two nonlinear equations based on mass and energy conservation are solved for burned gas shells. These two equations are solved at each time step for two unknowns, the burned gas temperature of the outermost shell and the burned mass fraction at each time step [72]. Isentropic relation is used to update temperature. At each time step the flame radius is calculated as a function of time from the BMF. The procedure is continued till the end of combustion. Metghalchi and coworkers [31, 42, 69, 72] determined S_u according to the following relationship

$$S_u = \frac{m_0}{\rho_u A_f}\frac{dx}{dt}, \tag{11}$$

here $A_f = 4\pi R_f^2$ is the flame front area. The above equation can be obtained by Substituting Eq. (7) into (3). The heat transfer to the wall can be considered in the multi-zone model by introducing the boundary layer displacement thickness [72]. The total heat transfer to the wall for CH_4/air was found to be within 1 % and thereby is negligible [72]. The readers are referred to Refs. [44, 71] for more details about the multi-zone model. While in multi-zone model $x = x(P)$ is found by solving the conservation equations for different shells in burned mass region, in two-zone model an explicit correlation is used for $x = x(P)$. Choosing an appropriate formulation to find $x = x(P)$ is crucial for accurate measurement of S_u in CVM.

A specific procedure can be prescribed to determine S_u in CVM. It consists of two steps: (1) to solve the conservation equations to obtain BMF for different shells (for multi-zone model) or to choose a correlation $x = x(P)$ (for two-zone model); (2) to choose an appropriate formulation to evaluate S_u. These two steps will be discussed respectively in the next two subsections.

4.3 Relationship between burned mass fraction and pressure

Using multi-zone model, Lewis and von Elbe [49] proposed the following relationship between burned mass fraction (BMF) and pressure:

$$x(P) = 1 - \frac{RT_0(P_e - P)/P_0}{RT_u(\gamma_b - \gamma_u)/(\gamma_u - 1) + (\gamma_b - 1)k},$$

with

$$k = \left(\frac{n_b}{n_u}\right)C_{pb}T_b - C_{pu}T_u, \tag{12}$$

in which R is the universal gas constant; P_e is the final pressure; γ_b and γ_u are the heat capacity ratio of burned and unburned gases; C_{pb} and C_{pu} are molar heat capacity of burned and unburned gases; n_b and n_u are number of moles per unit mass of burned and unburned gas; and T_b varies for different burning annular shells. Although k cannot be directly computed or measured, it can be computed at the limiting case of $x(P = P_0) = 0$:

$$k = \frac{RT_0}{(\gamma_b - 1)}\left(\frac{P_e}{P_0} - \frac{\gamma_b - 1}{\gamma_u - 1}\right). \tag{13}$$

Later Lewis and von Elbe [103] proposed the following linear relationship between BMF and pressure:

$$x = \frac{(P - P_0)}{(P_e - P_0)}. \tag{14}$$

This linear relationship is popularly used in CVM (e.g., [28, 51, 67, 68]). Grumer et al. [104] proposed a relation which was claimed to be more accurate than the linear one of Lewis and von Elbe [103]. However the relation of Grumer et al. [104] is valid only for the restricted region of $P < 1.1P_0$. O'Donovan and Rallis [47] proposed the following relation which works for the whole combustion period:

$$x(P) = \frac{(\bar{T}_e/\bar{T}_b)\left(P/P_0 - (P/P_0)^{(\gamma_u - 1)/\gamma_u}\right)}{P_e/P_0 - (\bar{T}_e/\bar{T}_b)(P/P_0)^{(\gamma_u - 1)/\gamma_u}}. \tag{15}$$

In which $\bar{T}_b$ and $\bar{T}_e$ are respectively the mass-averaged burned gas temperature and its value at the end of combustion. Since it is difficult to determine these two temperatures, it was assumed that $\bar{T}_b = \bar{T}_e$ and obtained the following equation [46]:

$$x(P) = \frac{P - P_0(P/P_0)^{(\gamma_u - 1)/\gamma_u}}{P_e - P_0(P/P_0)^{(\gamma_u - 1)/\gamma_u}}. \tag{16}$$

Nagy et al. [105] presented a correlation to measure laminar flame speed in which $x = x(P)$ was not used explicitly. Luijten et al. [43] derived an explicit expression for $x = x(P)$ from the relation of Nagy et al. [105]:

$$x(P) = \frac{P^{1/\gamma_u} - P_0^{1/\gamma_u}}{P_e^{1/\gamma_b}P^{(1/\gamma_u - 1/\gamma_b)} - P_0^{1/\gamma_u}}. \tag{17}$$

Rallis and Garfoth [8], suggested the following equation in their review paper:

$$x(P) = \frac{\alpha\left[(P/P_0)^{1/\gamma_u} - 1\right]}{(P/P_0)^{1/\gamma_u} - \alpha}, \quad \text{with}$$
$$\alpha = \frac{\rho_b^0}{\rho_0} + \frac{(1 - \rho_b^0/\rho_0)(P/P_0 - 1)}{(P_e/P_0 - 1)}. \tag{18}$$

As mentioned before, the linear relationship between BMF and pressure in Eq. (14) is popularly used. However, Luijten et al. [43] found that the linear relationship has noticeable error and they proposed an analytical correlation which was claimed to be as accurate as the one obtained from multi-zone model:

$$x = \frac{P - P_0 f(P)}{P_e - P_0 f(P)}, \text{ with}$$
$$f(P) = \frac{\gamma_b - 1}{\gamma_u - 1} + \frac{\gamma_u - \gamma_b}{\gamma_u - 1}\left(\frac{P}{P_0}\right)^{(\gamma_u - 1)/\gamma_u}. \quad (19)$$

Luijten et al. [43] suggested that Eq. (19) can be obtained by substituting Eq. (13) into (12) without the requisite of any simplifying assumption which was originally used by Lewis and von Elbe [49]. It is noted that both γ_u and γ_b are used in the above equation. According to our DNS of stoichiometric CH_4/air at NTP, γ_b changes from 1.27 to 1.25 during the spherical flame propagation. Our analysis indicates that the burned mass fraction, x, in Eq. (19) is very sensitive to the value of γ_b. Usually the frozen heat capacity ratio, $\gamma_{b,frozen}$, is used and it is about 1.25 for hydrocarbon/air mixtures. However, chemical equilibrium shifting in burned gas substantially affects the value of γ_b and a value of $\gamma_{b,shift} = 1.17$ was suggested in Ref. [106] for hydrocarbon/air mixtures. Unfortunately, there is no prescribed method to evaluate $\gamma_{b,shift}$. We used an iterative method to relate $\gamma_{b,shift}$ to $\gamma_{b,frozen}$ for different initial conditions of CH4/air mixture and proposed the following empirical correlation:

$$\gamma_{b,shift} = \frac{\gamma_b + 8}{8}. \quad (20)$$

A correlation of $\gamma_{b,shift} = (\gamma_b + 1)/2$ is recently suggested by Omari and Tartakovsky [107] to be used in Eq. (19). Our comparative analysis by DNS shows that Eq. (20) and $\gamma_{b,shift} = 1.17$ result in more accurate BMF comparing to Ref. [107]. As mentioned before, it is difficult to evaluate the average temperature in Eq. (15). Oancea et al. [108] proposed the following approximation for $\bar{T}_e/\bar{T}_b$:

$$\frac{\bar{T}_e}{\bar{T}_b} = \left(\frac{P_e}{P}\right)^{(\gamma^* - 1)/\gamma^*}, \text{ with } \gamma^* = \ln\left(\frac{P_e}{P_0}\left(1 - \frac{T_{f,p}}{T_{f,v}}\right)\right), \quad (21)$$

in which $T_{f,p}$ and $T_{f,v}$ are respectively the adiabatic flame temperature of isobaric and isochoric combustion at $P = P_0$. Razus et al. [63] suggested to use data at $P > 1.5P_0$ so that the influence of flame stretch and curvature on S_u can be circumvented.

The correlations presented to find BMF are summarized in Table 2. The performance of these correlations for $x = x(P)$ is compared in Fig. 7 based on the accurate results obtained from DNS using A-SURF [58, 85, 93, 97, 109–112]. The 1D spherical combustion chamber with the radius of $R_W = 5$ cm was used in simulation. We considered stoichiometric methane/air mixture at NTP and the methane oxidation mechanism GRI-Mech. 3.0 [82] was used. In simulation the flame front was defined as the position of maximum heat release rate and BMF was calculated using $x = 1 - m_u/m_0$ in which m_u is the total mass before the flame front (i.e., mass within $R_f < r < R_W$).

In Eq. (17), $\gamma_{b,shift}$ from Eq. (20) is used to increase the accuracy. It is observed that the discrepancy of different correlations is maximum in the midrange pressures. The most accurate result is obtained by using Eq. (19) in which Eq. (20) is used for γ_b. Similar suggestion was made by Omari and Tartakovsky [107]. Equations (19) and (21) have almost the same accuracy. The most deviated results

Table 2 Equations used to determine the burned mass fraction, x

Group	Correlation	Year	Eq. nos.
Lewis and von Elbe [103]	$x = \frac{(P-P_0)}{(P_e-P_0)}$	1951	(14)
O'Donovan and Rallis [47]	$x(P) = \frac{(\bar{T}_e/\bar{T}_b)\left(P/P_0-(P/P_0)^{(\gamma_u-1)/\gamma_u}\right)}{P_e/P_0-(\bar{T}_e/\bar{T}_b)(P/P_0)^{(\gamma_u-1)/\gamma_u}}$	1959	(15)
Rallis and Tremeer [46]	$x(P) = \frac{P-P_0(P/P_0)^{(\gamma_u-1)/\gamma_u}}{P_e-P_0(P/P_0)^{(\gamma_u-1)/\gamma_u}}$	1963	(16)
Nagy et al. [105]	$x(P) = \frac{P^{1/\gamma_u}-P_0^{1/\gamma_u}}{P_e^{1/\gamma_b}P^{(1/\gamma_u-1/\gamma_b)}-P_0^{1/\gamma_u}}$	1969	(17)
Rallis and Garforth [8]	$x(P) = \frac{\alpha\left[(P/P_0)^{1/\gamma_u}-1\right]}{(P/P_0)^{1/\gamma_u}-\alpha}$, $\alpha = \frac{\rho_b^0}{\rho_0} + \frac{\left(1-\rho_b^0/\rho_0\right)(P/P_0-1)}{(P_e/P_0-1)}$	1980	(18)
Luijten et al. [43]	$x = \frac{P-P_0f(P)}{P_e-P_0f(P)}$, $f(P) = \frac{\gamma_b-1}{\gamma_u-1} + \frac{\gamma_u-\gamma_b}{\gamma_u-1}\left(\frac{P}{P_0}\right)^{(\gamma_u-1)/\gamma_u}$	2009	(19)
Oancea et al. [108]	$x(P) = \frac{(\bar{T}_e/\bar{T}_b)\left(P/P_0-(P/P_0)^{(\gamma_u-1)/\gamma_u}\right)}{P_e/P_0-(\bar{T}_e/\bar{T}_b)(P/P_0)^{(\gamma_u-1)/\gamma_u}}$, $\frac{\bar{T}_e}{\bar{T}_b} = \left(\frac{P_e}{P}\right)^{(\gamma^*-1)/\gamma^*}$, $\gamma^* = \ln\left(\frac{P_e}{P_0}\left(1-\frac{T_{f,p}}{T_{f,v}}\right)\right)$	1994	(15), (21)
Current work update, the value of $\gamma_{b,shift}$ is close to 1.17 as suggested in Ref. [106]	$x = \frac{P-P_0f(P)}{P_e-P_0f(P)}$, $f(P) = \frac{\gamma_b-1}{\gamma_u-1} + \frac{\gamma_u-\gamma_b}{\gamma_u-1}\left(\frac{P}{P_0}\right)^{(\gamma_u-1)/\gamma_u}$, $\gamma_{b,shift} = \frac{\gamma_b+8}{8}$	2016	(19), (20)

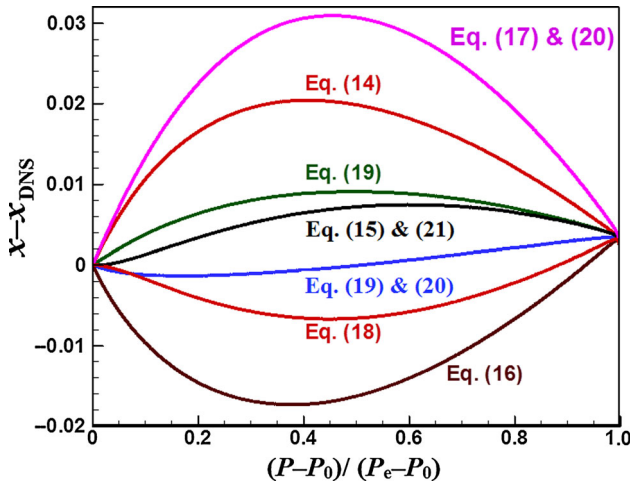

Fig. 7 (Color online) Relative error in BMF predicted by different correlations as a function of normalized pressure for stoichiometric CH_4/air mixture initially at NTP

are obtained by Eq. (16) and the combination of Eqs. (17) and (20); it is mainly because of the simplifying assumptions used to derive these relations which are discussed earlier.

4.4 Equations for the determination of S_u

Deriving a suitable correlation or choosing the most appropriate one to determine S_u from pressure evolution, $P = P(t)$, recorded in experiments is crucial in CVM. The first equation for determining S_u in CVM was proposed by Lewis and von Elbe [49]:

$$S_u = \frac{dR_i}{dt}\left(\frac{R_i}{R_b}\right)^2\left(\frac{P}{P_0}\right)^{-1/\gamma_u}, \tag{22}$$

in which R_i and R_b are respectively the radii of a shell before and after combustion, P the instantaneous pressure, P_0 the initial pressure of premixture, and γ_u the specific heat capacity ratio of unburned gas. However, Lewis and von Elbe [49] used the two-zone model and didn't include the temperature gradient in the burned gas region. Fiock and Marvin [48] proposed Eq. (6) to determine S_u, which was used for $R_f/R_W > 25$ % [113]. Eschenbach and Agnew [114] derived an equation only valid for slow burning mixtures (flame speed smaller than one tenth of sound speed) and for pressure rise <7 % of the initial pressure. O'Donovan and Rallis [47] proposed Eq. (10) to determine S_u.

Rallis and Tremeer [46] derived the following equation:

$$S_b = \frac{\rho_0}{\rho_u}\left[\alpha\frac{dR_f}{dt} + \frac{R_f}{3}\frac{d\alpha}{dP}\frac{dP}{dt}\right], \tag{23}$$

in which S_b is the flame speed with respect to burned gas. α is defined as

$$\alpha = \frac{\bar{\rho}_b}{\rho_0} = \frac{\bar{M}_b}{M_0}\frac{T_0}{\bar{T}_b}\frac{P}{P_0} = \frac{\bar{M}_b}{\bar{M}_e}\frac{\bar{T}_e}{\bar{T}_b}\frac{P}{P_e}, \tag{24}$$

where M is molecular weight. In practice the variation in $\bar{M}_b$ and $\bar{T}_b$ is small so the approximation of $d\alpha/dP = 1/P_e$ was suggested in Ref. [46]. Nevertheless, it is still difficult to evaluate α. Nagy et al. [105] proposed to assume constant and equal specific heat capacity ratio of burned and unburned gas. As shown in Ref. [43], these assumptions results in low accuracy.

Stone et al. [30, 44, 73–75] used an extended version of Eq. (22) by the multi-zone model to determine S_u:

$$S_u = \left(\frac{dP}{dt}\right)\left(\frac{dR_{i,n}}{dP}\right)\left(\frac{R_{i,n}}{R_{b,n}}\right)^2\left(\frac{P_0}{P}\right)^{1/\gamma_u},$$
$$R_{i,n} = x^{1/3}R_W, R_{b,n} = R_W\left[1-(1-x)\left(\frac{P_{u,n-1}}{P_{n-1}}\right)^{1/\gamma_{u,n-1}}\right]^{1/3}, \tag{25}$$

in which $R_{i,n}$ and $R_{b,n}$ are position of elemental shell before burning and after burning in shell number n which are function of pressure. These radii were calculated by the in house code (BOMB program) in which multi-zone model was used [30].

In CVM, usually the following power law is used to express the laminar flame speed S_u as a function of temperature T_u and pressure P [2, 27, 29, 42, 68, 76, 78]

$$S_u = S_{u,0}\left(\frac{T_u}{T_{u,0}}\right)^{\alpha}\left(\frac{P}{P_0}\right)^{\beta}, \tag{26}$$

where $S_{u,0}$ is the laminar flame speed at the reference temperature and pressure of $T_{u,0}$ and P_0; and α, β are exponential constants. In CVM, $S_{u,0}$, α and β are obtained from data fitting. Therefore, the laminar flame speed at $T_{u,0}$ and P_0 can also be obtained in CVM. Metghalchi and Keck [60] found that the above power-law works accurately only for pressure above 2 atm. The main drawback of using power law is the requisite of extrapolation or data fitting.

Table 1 summarizes the main groups working on S_u measurement using the CVM and their methods to determine S_u. Table 1 indicates that different groups used different S_u correlations. However, to our knowledge, the performance of these correlations were not compared in the literature. According to previous discussions, the main correlations to obtain S_u are Eqs. (6), (10) and (22). Saeed and Stone [44] extended the definition of Eq. (22) to include temperature gradient in burned gas in Eq. (25). The performance of these correlations in terms of evaluating S_u was compared for stoichiometric CH_4/air initially at NTP and the results were shown in Fig. 8. These results were based on pressure history, $P = P(t)$, from one-dimensional simulation of spherical flame propagation in a closed

chamber. Besides, the laminar flame speeds predicted by the PREMIX code [81] were plotted in Fig. 8 for comparison. In Fig. 8, "direct" means that dR_f/dt is directly calculated from flame front history, $R_f = R_f(t)$, from simulation using A-SURF; while "indirect" means that dR_f/dt is calculated from pressure history and BMF using Eq. (9). We did not use experimental data since in experiments the effects of radiation, ignition, flame instability and mixture preparation cannot be completely circumvented. When the simulation data are used, these effects are prevented and thereby the results are only affected by the correlations used to evaluate S_u. The pressure region show in Fig. 8 is from 2.5 to 6.5 atm, in which the stretch effect is negligible [40]. All the correlations yield very similar S_u and the difference among is within 1.5 cm/s. This shows the importance of BMF: inserting the same BMF in different S_u relations can reduce the discrepancy between them. Figure 8 shows that, at elevated pressures Eq. (6) is more accurate than Eqs. (10) and (25). However, Eq. (6) is a subtraction of two large terms of similar magnitude. Besides, many groups who perform CVM experiments donot use optical access in combustion chamber and flame front monitoring is not possible [40, 42, 78]. Therefore, Eq. (6) is not popularly used in experiment. Similar suggestion was also made by Omari and Tartakovsky [107] based on their experimental results.

The power law is used to obtain the laminar flame speed at NTP and the results are plotted in Fig. 9 as a function of

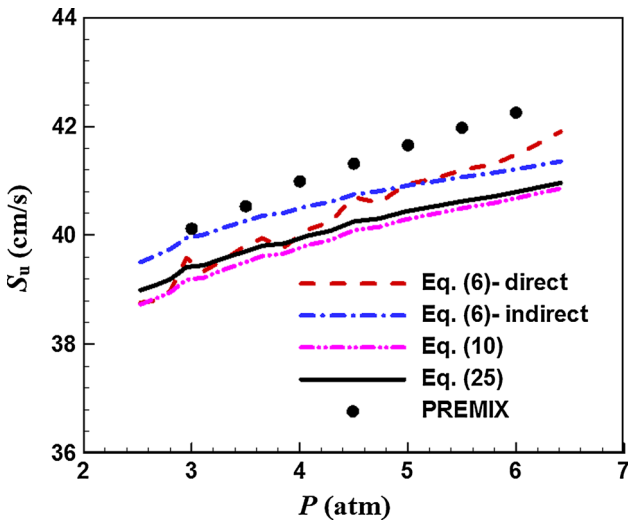

Fig. 8 (Color online) Laminar flame speed calculated from different correlations as a function of pressure for stoichiometric CH_4/air mixture initially at NTP. Red dashed line: Eq. (6) by Fiock and Marvin [48] in which dR_f/dt is directly calculated by A-SURF; blue dash-dotted line: Eq. (6) by Fiock and Marvin [48] in which dR_f/dt is from Eq. (9); pink dash-dot-dotted line: Eq. (10) by Rallis and O'donovan [47]; black line: Eq. (25) by Saeed and Stone [30]; symbols: S_u^0 measured with PREMIX

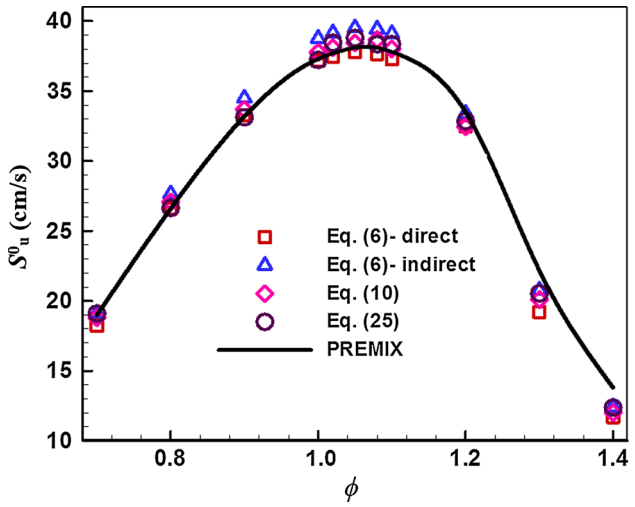

Fig. 9 (Color online) Laminar flame speed at $T_u = 298$ K and $P = 1$ atm calculated from different correlations as a function of equivalence ratio for CH_4/air mixture initially at NTP. Red squares: Eq. (6) by Fiock and Marvin [48] in which dR_f/dt is directly calculated by A-SURF; blue triangles: Eq. (6) by Fiock and Marvin [48] in which dR_f/dt is from Eq. (9); pink diamonds: Eq. (10) by Rallis and O'donovan [47]; purple circles: Eq. (25) by Saeed and Stone [30]; the solid black line: results from PREMIX

equivalence ratio. Besides, the laminar flame speeds predicted by the PREMIX are shown together for comparison. Low scatter is observed in fuel–leaner mixtures. Compared to PREMIX results, all correlations under-predict the flame speed for fuel-rich mixtures. The scatter between different correlations in near stoichiometric conditions is higher than fuel–lean cases. Comparison in Figs. 8 and 9 indicates that high sensitivity of power law (due to the large slope in S_u–P curve) increases the discrepancy among results obtained from different correlations. To quantify the discrepancy, Fig. 10 shows the results normalized by the value predicted by PREMIX. It is observed that Eqs. (10) and (25) are more accurate than Eq. (6) after extrapolation. It is noted that the error from extrapolation may cancel the error from using different correlations. However the definition of Eq. (10) is much simpler compared to Eq. (25). Therefore, Eq. (10) is recommended to be used for CVM when $S_{u,0}$ is required.

Figrue 11 shows S_u determined by Eq. (10) and different correlations for BMF already compared in Fig 7. Because of their high discrepancy shown in Fig. 7, Eqs. (16) and (17) were not considered in Fig. 11. The deviation between results from different formulations and those from A-SURF is shown to be large at low and high pressure regions. The maximum deviation is observed from Eq. (14). It is noted that the expression for BMF does not have significant effect on S_u for $P > 2.5P_0$. Extrapolation based on Eq. (26) was conducted to get $S_{u,0}$ at $T_0 = 298$ K and $P_0 = 1$ atm as shown by solid lines in Fig. 11. It is

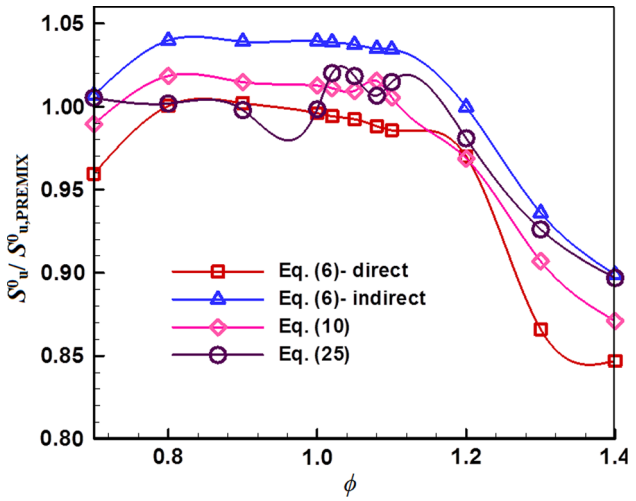

Fig. 10 (Color online) Deviation of S_u^0 calculated by different correlations from that predicted by simulation for CH_4/air mixture initially at NTP

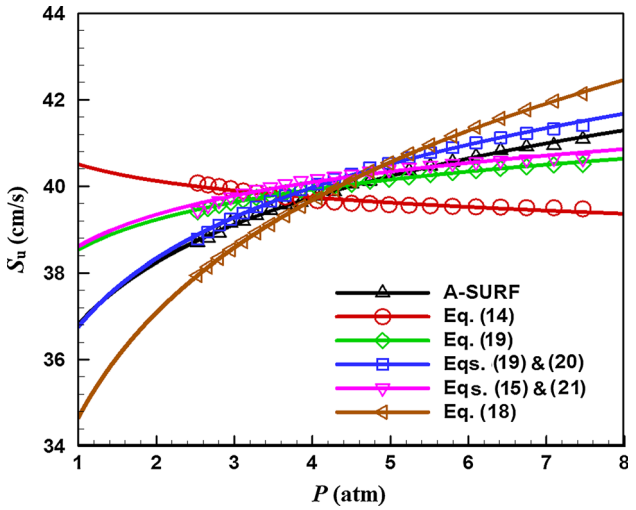

Fig. 11 (Color online) S_u determined by Eq. (10) and different correlations (indicated in the figure) for BMF for stoichiometric CH_4/air mixture initially at NTP

seen that the expression for BMF has significant impact on $S_{u,0}$. The error of using Eq. (14) exceeds 10 % and the error of using Eqs. (18), (19) and (21) is around 5 %. The combination of Eqs. (19) and (20) is as accurate as A-SURF result, which shows the importance of BMF when extrapolation is performed to obtain $S_{u,0}$ at initial temperature and pressure.

5 Concluding remarks

The constant-volume propagating spherical flame method (CVM) for laminar flame speed measurement is reviewed. It is found that there are still large discrepancies in S_u^0 measured by different groups for the same mixture using the CVM, at nearly the same condition. Since S_u^0 data with large discrepancies cannot be used to optimize chemical models, efforts are still needed to improve the accuracy of S_u^0 measurement. The possible sources of uncertainty in S_u^0 measured by CVM are discussed and special attention is devoted to the error encountered in data processing. Different correlations among pressure, temperature and flame speed, which are used by different researchers to obtain S_u^0, are summarized and the performance of these correlations are examined. It is shown that the combination of Eqs. (19) and (20) is the most accurate in terms of evaluating the dependency of BMF on pressure. For laminar flame speed, Eqs. (6), (10) and (25) have similar accuracy. Because of the simplicity of Eq. (10), it is recommended to be used for CVM. Besides, Eq. (6) is the subtraction of two large terms of similar magnitude and usually there is no availability of optical access in CVM. Therefore, Eq. (10) instead of (6) is recommended.

Further studies are still needed in order to obtain accurate laminar flame speed from CVM. The possible areas of future research on CVM are

(1). In CVM, it is assumed that no dissociation or pre-flame reaction occurs in unburned gas. Large hydrocarbon fuels has low-temperature chemistry and pre-flame reaction might occur in unburned gas, especially at elevated initial temperature and pressure. Therefore, it is necessary to check the validity of this assumption and to examine the influence of pre-flame reaction on the accuracy of laminar flame speed measured by CVM.

(2). In all the correlations used in CVM for BMF and laminar flame speed, radiation effects were not comprehensively examined though several studies considered radiation effects. For highly-diluted mixtures with relatively low flame speed, the radiation effects might be important. Besides, for CO_2 or H_2O diluted mixtures, radiation absorption might also affect the accuracy of laminar flame speed measured by CVM. Therefore, the influence of radiation on the accuracy of the correlations used in CVM still needs further study.

(3). In data processing, different ranges of pressure history are used by different researchers and it is not clear how the pressure history range affects the accuracy of laminar flame speed measured by CVM. Besides, different researchers used different pressure regions in which the flame is stretch free. Though in Ref. [40] it was proposed to only use pressure history at $P > 2.5P_0$, the investigation was performed only for a few cases. Further studies for different fuels and for broad range of initial conditions are needed.

Acknowledgments The work was supported by the National Natural Science Foundation of China (51322602).

Conflict of interest All authors declare that they have no conflict of interest.

References

1. Andrews GE, Bradley D (1972) Determination of burning velocities: a critical review. Combust Flame 18:133–153
2. Metghalchi H, Keck JC (1980) Laminar burning velocity of propane–air mixtures at high temperature and pressure. Combust Flame 38:143–154
3. Law CK (2006) Combustion physics. Cambridge University Press, New York
4. Law CK, Sung CJ, Wang H et al (2003) Development of comprehensive detailed and reduced reaction mechanisms for combustion modeling. AIAA J 41:1629–1646
5. Dooley S, Won SH, Chaos M et al (2010) A jet fuel surrogate formulated by real fuel properties. Combust Flame 157:2333–2339
6. Ranzi E, Frassoldati A, Grana R et al (2012) Hierarchical and comparative kinetic modeling of laminar flame speeds of hydrocarbon and oxygenated fuels. Prog Energy Combust Sci 38:468–501
7. Peters N (2000) Turbulent combustion. Cambridge University Press, Cambridge
8. Rallis CJ, Garforth AM (1980) The determination of laminar burning velocity. Prog Energy Combust Sci 6:303–329
9. Egolfopoulos FN, Hansen N, Ju Y et al (2014) Advances and challenges in laminar flame experiments and implications for combustion chemistry. Prog Energy Combust Sci 43:36–67
10. Lewis B, Von Elbe G (2012) Combustion, flames and explosions of gases. Elsevier, London
11. Tsuji H (1982) Counterflow diffusion flames. Prog Energy Combust Sci 8:93–119
12. Wu CK, Law CK (1985) On the determination of laminar flame speeds from stretched flames. Symp Int Combust Proc 20:1941–1949
13. Egolfopoulos FN, Cho P, Law CK (1989) Laminar flame speeds of methane–air mixtures under reduced and elevated pressures. Combust Flame 76:375–391
14. Huang Y, Sung CJ, Eng JA (2004) Laminar flame speeds of primary reference fuels and reformer gas mixtures. Combust Flame 139:239–251
15. Levy A, Weinberg F (1958) Optical flame structure studies: some conclusions concerning the propagation of flat flames. Symp Int Combust Proc 7:296–303
16. Van Maaren A, Thung DS, De Goey LRH (1994) Measurement of flame temperature and adiabatic burning velocity of methane/air mixtures. Combust Sci Technol 96:327–344
17. Qin X, Ju YG (2005) Measurements of burning velocities of dimethyl ether and air premixed flames at elevated pressures. Proc Combust Inst 30:233–240
18. Aung KT, Hassan MI, Faeth GM (1997) Flame stretch interactions of laminar premixed hydrogen/air flames at normal temperature and pressure. Combust Flame 109:1–24
19. Brown MJ, McLean IC, Smith DB et al (1996) Markstein lengths of CO/H_2/air flames, using expanding spherical flames. Symp Int Combust Proc 26:875–881
20. Tse SD, Zhu DL, Law CK (2000) Morphology and burning rates of expanding spherical flames in H_2/O_2/inert mixtures up to 60 atmospheres. Proc Combust Inst 28:1793–1800
21. Kwon S, Tseng LK, Faeth GM (1992) Laminar burning velocities and transition to unstable flames in $H_2/O_2/N_2$ and $C_3H_8/O_2/N_2$ mixtures. Combust Flame 90:230–246
22. Aung KT, Hassan MI, Faeth GM (1998) Effects of pressure and nitrogen dilution on flame/stretch interactions of laminar premixed $H_2/O_2/N_2$ flames. Combust Flame 112:1–15
23. Bradley D, Hicks RA, Lawes M et al (1998) The measurement of laminar burning velocities and Markstein numbers for iso-octane–air and iso-octane–*n*-heptane–air mixtures at elevated temperatures and pressures in an explosion bomb. Combust Flame 115:126–144
24. Huang Z, Zhang Y, Zeng K et al (2006) Measurements of laminar burning velocities for natural gas–hydrogen–air mixtures. Combust Flame 146:302–311
25. Chen Z, Qin X, Ju Y et al (2007) High temperature ignition and combustion enhancement by dimethyl ether addition to methane–air mixtures. Proc Combust Inst 31:1215–1222
26. Halter F, Chauveau C, Djebaïli-Chaumeix N et al (2005) Characterization of the effects of pressure and hydrogen concentration on laminar burning velocities of methane–hydrogen–air mixtures. Proc Combust Inst 30:201–208
27. Takizawa K, Takahashi A, Tokuhashi K et al (2005) Burning velocity measurement of fluorinated compounds by the spherical-vessel method. Combust Flame 141:298–307
28. Bradley D, Mitcheson A (1976) Mathematical solutions for explosions in spherical vessels. Combust Flame 26:201–217
29. Hill P, Hung J (1988) Laminar burning velocities of stoichiometric mixtures of methane with propane and ethane additives. Combust Sci Technol 60:7–30
30. Saeed K, Stone CR (2004) Measurements of the laminar burning velocity for mixtures of methanol and air from a constant-volume vessel using a multizone model. Combust Flame 139:152–166
31. Parsinejad F, Arcari C, Metghalchi H (2006) Flame structure and burning speed of JP-10 air mixtures. Combust Sci Technol 178:975–1000
32. Huzayyin AS, Moneib HA, Shehatta MS et al (2008) Laminar burning velocity and explosion index of LPG–air and propane–air mixtures. Fuel 87:39–57
33. Smith FA (1948) Problems of stationary flames. Proc Combust Inst 1:206–219
34. Echekki T, Mungal MG (1991) Flame speed measurements at the tip of a slot burner: effects of flame curvature and hydrodynamic stretch. Symp Int Combust Proc 23:455–461
35. Law CK (1989) Dynamics of stretched flames. Symp Int Combust Proc 22:1381–1402
36. Simmons RF, Wolfhard HG (1957) Some limiting oxygen concentrations for diffusion flames in air diluted with nitrogen. Combust Flame 1:155–161
37. Botha JP, Spalding DB (1954) The laminar flame speed of propane/air mixtures with heat extraction from the flame. Proc Math Phys Eng Sci 225:71–96
38. de Goey LPH, van Maaren A, Quax RM (1993) Stabilization of adiabatic premixed laminar flames on a flat flame burner. Combust Sci Technol 92:201–207
39. Alekseev VA, Naucler JD, Christensen M et al (2015) Experimental uncertainties of the heat flux method for measuring burning velocities. Combust Sci Technol 188:853–894
40. Xiouris C, Ye T, Jayachandran J et al (2016) Laminar flame speeds under engine-relevant conditions: uncertainty quantification and minimization in spherically expanding flame experiments. Combust Flame 163:270–283
41. Mitu M, Razus D, Giurcan V et al (2015) Normal burning velocity and propagation speed of ethane–air: pressure and temperature dependence. Fuel 147:27–34

42. Moghaddas A, Eisazadeh-Far K, Metghalchi H (2012) Laminar burning speed measurement of premixed *n*-decane/air mixtures using spherically expanding flames at high temperatures and pressures. Combust Flame 159:1437–1443
43. Luijten CCM, Doosje E, de Goey LPH (2009) Accurate analytical models for fractional pressure rise in constant volume combustion. Int J Therm Sci 48:1213–1222
44. Saeed K, Stone CR (2004) The modelling of premixed laminar combustion in a closed vessel. Combust Theor Model 8:721–743
45. Iijima T, Takeno T (1986) Effects of temperature and pressure on burning velocity. Combust Flame 65:35–43
46. Rallis CJ, Tremeer GEB (1963) Equations for the determination of burning velocity in a spherical constant volume vessel. Combust Flame 7:51–61
47. O'Donovan KH, Rallis CJ (1959) A modified analysis for the determination of the burning velocity of a gas mixture in a spherical constant volume combustion vessel. Combust Flame 3:201–214
48. Fiock EF, Marvin CF (1937) The measurement of flame speeds. Chem Rev 21:367–387
49. Lewis B, von Elbe G (1934) Determination of the speed of flames and the temperature distribution in a spherical bomb from time-pressure explosion records. J Chem Phys 2:283–290
50. Stevens F (1923) A constant pressure bomb. NACA Technical Report, NACA-TR-176
51. Chen Z, Burke MP, Ju YG (2009) Effects of compression and stretch on the determination of laminar flame speeds using propagating spherical flames. Combust Theor Model 13: 343–364
52. Ellis O (1928) Flame movement in gaseous explosive mixtures. Fuel 7:245–252
53. Rubtsov NM, Troshin KY, Borisov AA et al (2011) Influence of inert and active additives on the initiation and propagation of laminar spherical flames in stoichiometric mixtures of methane, pentane, and hydrogen with air. Russ J Phys Chem B 5:57–66
54. Xiao H, Mao Z, An W et al (2014) Experimental and LES investigation of flame propagation in a hydrogen/air mixture in a combustion vessel. Chin Sci Bull 59:2496–2504
55. Bao XC, Liu FS (2011) Measurement and calculation of burning velocity of hydrogen–air laminar premixed flames. J Combust Sci Technol 17:407–413 (in Chinese)
56. Wang X, Zhang Z, Huang Z et al (2010) Experimental study on premixed combustion of spherically propagating methanol–air–nitrogen flames. Front Energy Power Eng China 4:223–233
57. Bradley D, Gaskell PH, Gu XJ (1996) Burning velocities, Markstein lengths, and flame quenching for spherical methane–air flames: a computational study. Combust Flame 104:176–198
58. Chen Z (2015) On the accuracy of laminar flame speeds measured from outwardly propagating spherical flames: methane/air at normal temperature and pressure. Combust Flame 162: 2442–2453
59. Zhou Z, Ai YH, Kong WJ (2013) Experimental investigation on laminar flame characteristics of syngas at elevated pressures. J Eng Thermophys 34:1560–1564 (in Chinese)
60. Metghalchi H, Keck JC (1982) Burning velocities of mixtures of air with methanol, isooctane, and indolene at high pressure and temperature. Combust Flame 48:191–210
61. Kelley AP, Smallbone AJ, Zhu DL et al (2011) Laminar flame speeds of C_5 to C_8 *n*-alkanes at elevated pressures: experimental determination, fuel similarity, and stretch sensitivity. Proc Combust Inst 33:963–970
62. Santner J, Dryer FL, Ju Y (2013) The effects of water dilution on hydrogen, syngas, and ethylene flames at elevated pressure. Proc Combust Inst 34:719–726
63. Razus D, Brinzea V, Mitu M et al (2012) Burning velocity of propane–air mixtures from pressure-time records during explosions in a closed spherical vessel. Energy Fuels 26:901–909
64. Faghih M, Gou X, Chen Z (2016) The explosion characteristics of methane, hydrogen and their mixtures: a computational study. J Loss Prev Process Ind 40:131–138
65. Sharma SP, Agrawal DD, Gupta CP (1981) The pressure and temperature dependence of burning velocity in a spherical combustion bomb. Symp Int Combust Proc 18:493–501
66. Farrell J, Johnston R, Androulakis I (2004) Molecular structure effects on laminar burning velocities at elevated temperature and pressure. SAE technical paper, 2004-01-2936
67. Yates A, Burger V, Viljoen C (2012) A method for determining the laminar flame speed of jet fuels using combustion bomb pressure. Proc ASME Turbo Expo 2:41–51
68. Matsugi A, Shiina H, Takahashi A et al (2014) Burning velocities and kinetics of $H_2/NF_3/N_2$, $CH_4/NF_3/N_2$, and $C_3H_8/NF_3/N_2$ flames. Combust Flame 161:1425–1431
69. Moghaddas A, Bennett C, Rokni E et al (2014) Laminar burning speeds and flame structures of mixtures of difluoromethane (HFC-32) and 1,1-difluoroethane (HFC-152a) with air at elevated temperatures and pressures. HVAC&R Res 20:42–50
70. Eisazadeh-Far K, Moghaddas A, Al-Mulki J et al (2011) Laminar burning speeds of ethanol/air/diluent mixtures. Proc Combust Inst 33:1021–1027
71. Rahim F, Elia M, Ulinski M et al (2002) Burning velocity measurements of methane–oxygen–argon mixtures and an application to extend methane–air burning velocity measurements. Int J Engine Res 3:81–92
72. Elia M, Ulinski M, Metghalchi H (2001) Laminar burning velocity of methane–air–diluent mixtures. J Eng Gas Turb Power 123:190–196
73. Hinton N, Stone R (2014) Laminar burning velocity measurements of methane and carbon dioxide mixtures (biogas) over wide ranging temperatures and pressures. Fuel 116:743–750
74. Marshall SP, Taylor S, Stone CR et al (2011) Laminar burning velocity measurements of liquid fuels at elevated pressures and temperatures with combustion residuals. Combust Flame 158:1920–1932
75. Marshall SP, Stone R, Heghes C et al (2010) High pressure laminar burning velocity measurements and modelling of methane and *n*-butane. Combust Theor Model 14:519–540
76. Stone R, Clarke A, Beckwith P (1998) Correlations for the laminar-burning velocity of methane/diluent/air mixtures obtained in free-fall experiments. Combust Flame 114:546–555
77. Clarke A, Stone R, Beckwith P (1995) Measuring the laminar burning velocity of methane/diluent/air mixtures within a constant-volume combustion bomb in a micro-gravity environment. J Inst Energy 68:130–136
78. Mitu M, Razus D, Giurcan V et al (2014) Experimental and numerical study of laminar burning velocity of ethane–air mixtures of variable initial composition, temperature and pressure. Energy Fuels 28:2179–2188
79. Giurcan V, Razus D, Mitu M et al (2014) Numerical study of the laminar flame propagation in ethane–air mixtures. Cent Eur J Chem 12:391–402
80. Sepljarsky B, Naboko I, Troshin KY et al (2014) Flame propagation regimes at combustion of lean hydrogen–air mixtures in the presence of additives at central spark initiation at atmospheric pressure. GJSFR B 14:19–29
81. Kee RJ, Grcar J, Smooke M et al (1985) PREMIX: a fortran program for modeling steady laminar one-dimensional premixed flames. Sandia report, SAND85-8240
82. Smith G, Golden D, Frenklach M et al (1999) The GRI-Mech 3.0 chemical kinetic mechanism. http://combustion.berkeley.edu/gri-mech/

83. Santner J, Haas FM, Dryer FL et al (2015) High temperature oxidation of formaldehyde and formyl radical: a study of 1,3,5-trioxane laminar burning velocities. Proc Combust Inst 35:687–694
84. Li X, You X, Wu F et al (2015) Uncertainty analysis of the kinetic model prediction for high-pressure H_2/CO combustion. Proc Combust Inst 35:617–624
85. Chen Z, Burke MP, Ju YG (2009) Effects of Lewis number and ignition energy on the determination of laminar flame speed using propagating spherical flames. Proc Combust Inst 32:1253–1260
86. Kim HH, Won SH, Santner J et al (2013) Measurements of the critical initiation radius and unsteady propagation of *n*-decane/air premixed flames. Proc Combust Inst 34:929–936
87. Ronney PD, Wachman HY (1985) Effect of gravity on laminar premixed gas combustion I: flammability limits and burning velocities. Combust Flame 62:107–119
88. Qiao L, Gu Y, Dahm WJA et al (2007) Near-limit laminar burning velocities of microgravity premixed hydrogen flames with chemically-passive fire suppressants. Proc Combust Inst 31:2701–2709
89. Bradley D, Lawes M, Liu K et al (2007) Laminar burning velocities of lean hydrogen–air mixtures at pressures up to 1.0 MPa. Combust Flame 149:162–172
90. Jomaas G, Law CK, Bechtold JK (2007) On transition to cellularity in expanding spherical flames. J Fluid Mech 583:1–26
91. Bonhomme A, Selle L, Poinsot T (2013) Curvature and confinement effects for flame speed measurements in laminar spherical and cylindrical flames. Combust Flame 160:1208–1214
92. Burke MP, Chen Z, Ju Y et al (2009) Effect of cylindrical confinement on the determination of laminar flame speeds using outwardly propagating flames. Combust Flame 156:771–779
93. Chen Z (2010) Effects of radiation and compression on propagating spherical flames of methane/air mixtures near the lean flammability limit. Combust Flame 157:2267–2276
94. Jayachandran J, Zhao R, Egolfopoulos FN (2014) Determination of laminar flame speeds using stagnation and spherically expanding flames: molecular transport and radiation effects. Combust Flame 161:2305–2316
95. Chen Z, Qin M, Xu B et al (2007) Studies of radiation absorption on flame speed and flammability limit of CO_2 diluted methane flames at elevated pressures. Proc Combust Inst 31:2693–2700
96. Santner J, Haas FM, Ju YG et al (2014) Uncertainties in interpretation of high pressure spherical flame propagation rates due to thermal radiation. Combust Flame 161:147–153
97. Yu H, Han W, Santner J et al (2014) Radiation-induced uncertainty in laminar flame speed measured from propagating spherical flames. Combust Flame 161:2815–2824
98. Beeckmann J, Chaumeix N, Dagaut P et al (2013) Collaborative study for accurate measurements of laminar burning velocity. Proc Europ Combust Meet P-76
99. Chen Z (2016) Effects of radiation absorption on spherical flame propagation and radiation-induced uncertainty in laminar flame speed measurement. Proc Combust Inst. doi:10.1016/j.proci.2016.05.003
100. Dahoe AE (2005) Laminar burning velocities of hydrogen–air mixtures from closed vessel gas explosions. J Loss Prev Process Ind 18:152–166
101. Ma Q, Zhang Q, Chen J et al (2014) Effects of hydrogen on combustion characteristics of methane in air. Int J Hydrog Energy 39:11291–11298
102. Salzano E, Cammarota F, Di Benedetto A et al (2012) Explosion behavior of hydrogen–methane/air mixtures. J Loss Prev Process Ind 25:443–447
103. Lewis B, von Elbe G (1951) Combustion, flames and explosions of gases. Academic Press, New York
104. Grumer J, Cook EB, Kubala TA (1959) Considerations pertaining to spherical-vessel combustion. Combust Flame 3:437–446
105. Nagy J, Conn JW, Verakis HC (1969) Explosion development in a spherical vessel, vol 7279. Department of the Interior, Bureau of Mines, Pittsburgh
106. van den Bulck E (2005) Closed algebraic expressions for the adiabatic limit value of the explosion constant in closed volume combustion. J Loss Prev Process Ind 18:35–42
107. Omari A, Tartakovsky L (2016) Measurement of the laminar burning velocity using the confined and unconfined spherical flame methods—a comparative analysis. Combust Flame 168:127–137
108. Oancea D, Razus D, Ionescu NI (1994) Burning velocity determination by spherical bomb technique. 1. A new model for burnt mass fraction. Rev Roum Chim 39:1187–1196
109. Chen Z (2011) On the extraction of laminar flame speed and Markstein length from outwardly propagating spherical flames. Combust Flame 158:291–300
110. Yu H, Chen Z (2015) End-gas autoignition and detonation development in a closed chamber. Combust Flame 162:4102–4111
111. Zhang W, Chen Z, Kong W (2012) Effects of diluents on the ignition of premixed H_2/air mixtures. Combust Flame 159:151–160
112. Dai P, Chen Z (2015) Supersonic reaction front propagation initiated by a hot spot in *n*-heptane/air mixture with multistage ignition. Combust Flame 162:4183–4193
113. Fiock EF, Marvin Jr CF, Caldwell FR et al (1940) Flame speeds and energy consideration for explosions in a spherical bomb. NACA Report no. 682
114. Eschenbach RC, Agnew JT (1958) Use of the constant-volume bomb technique for measuring burning velocity. Combust Flame 2:273–285